Impact of copper and iron binding properties on the anticancer activity of 8-hydroxyquinoline derived Mannich bases

Veronika F.S. Pape[a,†], Nóra V. May[b], G. Tamás Gál[b], István Szatmári[c], Flóra Szeri[a,§], Ferenc Fülöp[c], Gergely Szakács [a,f,*], Éva A. Enyedy[e,*]

[a] Institute of Enzymology, Research Centre for Natural Sciences, Hungarian Academy of Sciences, Magyar Tudósok körútja 2, H-1117 Budapest, Hungary

[b] Research Centre for Natural Sciences, Hungarian Academy of Sciences, Magyar Tudósok körútja 2, H-1117 Budapest, Hungary

[c] Institute of Pharmaceutical Chemistry and Stereochemistry Research Group of Hungarian Academy of Sciences, University of Szeged, Eötvös u. 6, H-6720 Szeged, Hungary

[d] Institute of Cancer Research, Medical University of Vienna, Borschkegasse 8a, A-1090 Vienna, Austria

[e] Department of Inorganic and Analytical Chemistry, Interdisciplinary Excellence Centre, University of Szeged, Dóm tér 7, H-6720 Szeged, Hungary

[†] Present address: Department of Physiology, Semmelweis University, Faculty of Medicine, Tűzoltó utca 37-47, H-1094 Budapest, Hungary

[§] Present address: Department of Dermatology and Cutaneous Biology, Sidney Kimmel Medical College, Thomas Jefferson University, 233 S. 10th Street, 19107 Philadelphia (PA), USA.

Table S1. Crystal data and structure refinement parameters for **Q-3**, **Q-4**·HCl·H_2O, [(Cu(H**Q-2**)$_2$)$_2$]·(CH_3OH)$_2$·Cl_4·(H_2O)$_2$, [Cu(**Q-3**)$_2$]·Cl_2 and [Cu(H**Q-4**)$_2$(CH_3OH)]·$ZnCl_4$·CH_3OH.

	Q-3	**Q-4**·HCl·H_2O	[(Cu(H**Q-2**)$_2$)$_2$]·(CH_3OH)$_2$·Cl_4·(H_2O)$_2$	[Cu(**Q-3**)$_2$]·Cl_2	[Cu(H**Q-4**)$_2$ (CH_3OH)]·$ZnCl_4$·CH_3OH)
CCDC number	1575107	1575108	1575109	1575110	1575111
Color/Shape	Colorless/ Chunk	Green/ Chunk	Green/ Chip	Orange/ Block	Green/ Block
Empirical formula	$C_{15}H_{18}N_2O$	$C_{17}H_{15}ClFN_2O$, Cl, H_2O	[(Cu($C_{14}H_{16}N_2O_2$)$_2$)$_2$] (CH_3OH)$_2$, (Cl)$_4$, (H_2O)$_2$	[Cu($C_{15}H_{17}N_2O$)$_2$] (Cl)$_2$	[Cu($C_{17}H_{14}ClFN_2O$)$_2$ (CH_3OH)] $ZnCl_4$, CH_3OH
Empirical formula	$C_{15}H_{18}N_2O$	$C_{17}H_{17}Cl_2FN_2O_2$	$C_{58}H_{76}Cl_4Cu_2N_8O_{12}$	$C_{30}H_{36}Cl_2CuN_4O_2$	$C_{36}H_{36}Cl_6CuF_2N_4O_4Zn$
Formula weight	242.31	371.22	1346.14	619.07	968.30
Temperature (K)	293(2)	293(2)	293(2)	293(2)	103(2)
Radiation, wavelength (Å)	Mo–Kα, 0.71073	Mo–Kα, 0.71073	Mo–Kα, 0.71073	Cu–Kα, 1.54187	Mo–Kα, 0.71073
Crystal system	orthorhombic	triclinic	monoclinic	monoclinic	triclinic
Space group	$P2_12_12_1$	P-1	$C2/c$	$P2_1$/n	P-1
Unit cell dimensions					
a, b, c (Å)	8.9362(7), 11.4735(10), 12.7458(11)	7.0220(3), 9.4970(5), 13.8230(6)	25.0347(19), 10.5428(7), 23.7514(17)	6.5336(2), 10.8906(4), 20.7810(7)	11.8498(12), 12.9144(11), 14.7891(17)
α, β, γ (°)	90, 90, 90.	95.430(2), 101.7900(10), 99.440(2).	90, 93.299(2), 90.	90, 91.408(2), 90.	76.700(3), 72.214(3), 67.890(3).
Volume (Å^3)	1306.8(2)	882.29(7)	6258.5(8)	1478.22(9)	1979.5(4)
Z/Z'	4/1	2/1	4/1	2/0.5	2/1
Density (calc.) (Mgm^{-3})	1.232	1.397	1.429	1.391	1.625
Abs. coeff. (mm^{-1})	0.078	0.389	0.916	2.973	1.602
F(000)	520	384	2808	646	982

Crystal size (mm)	0.3 ×0.3 × 0.25	0.50 × 0.50 × 0.30	0.25 × 0.25 × 0.25	0.25 × 0.1 × 0.1	0.25 × 0.25 × 0.1
Absorption correction	Numerical	Numerical	Numerical	Numerical	Multi-scan
Min. and max. transmission	0.9629, 1.0000	0.5925, 0.8590	0.7803, 0.8816	0.6680, 0.9085	0.6809, 1.0000
θ–range for data collection (°)	$3.197 \leq \theta \leq 27.397$	$3.017 \leq \theta \leq 27.436$	$3.116 \leq \theta \leq 25.326$	$7.057 \leq \theta \leq 58.881$	$3.076 \leq \theta \leq 27.481$
Index ranges	$-11 \leq h \leq 11$; $-14 \leq k \leq 14$; $-16 \leq l \leq 16$.	$-9 \leq h \leq 9$; $-12 \leq k \leq 12$; $-17 \leq l \leq 17$.	$-30 \leq h \leq 30$; $-12 \leq k \leq 12$; $-28 \leq l \leq 28$	$-7 \leq h \leq 5$; $-12 \leq k \leq 12$; $-22 \leq l \leq 20$	$-15 \leq h \leq 15$; $-16 \leq k \leq 16$; $-19 \leq l \leq 19$
No. reflections collected	41004	34133	69245	10477	60741
Completeness to 2θ	0.998	0.999	0.998	0.937	0.995
No. independent reflections (R_{int})	2956 (0.0457)	4014 (0.0357)	5720 (0.1184)	1982 (0.0704)	8981 (0.0582)
Reflections $I>2\sigma(I)$	2309	3421	4123	1233	6884
Refinement method	full-matrix least-squares on F^2				
Data / restraints / parameters	2956 /0 /168	4014 /0 /229	5720 /0 /398	1982 /0 /178	8981 /0 /497
Goodness-of-fit on $F2$	1.119	1.062	1.067	1.134	1.137
Final R indices [$I>2\sigma(I)$] R_1, wR_2	0.0527, 0.1402	0.0385, 0.1021	0.0683, 0.1236	0.0965, 0.1839	0.0454, 0.0983
R indices (all data) R_1, wR_2	0.0643, 0.1493	0.0452, 0.1078	0.1015, 0.1417	0.1542, 0.2482	0.0686, 0.1261
Max. and mean shift/esd	0.002; 0.000	0.000;0.000	0.000; 0.000	0.000; 0.000	0.001;0.000
Largest diff. peak and hole (e.Å^{-3})	0.170; -0.158	0.264; -0.175	0.578; -0.431	0.469; -0.459	0.738;-0.963

Table S2. Bond lengths (Å) and angles (°) in **Q-3**.

	Bond lengths (Å)		angles (°)
O1-C8	1.370(3)	C8-C7-C6	119.4(2)
C7-C6	1.411(4)	C6-C7-C9	120.3(2)
N10-C11	1.461(3)	C11-N10-C15	109.8(2)
N10-C15	1.477(4)	C2-N1-C8A	116.8(2)
N1-C8A	1.364(3)	N1-C8A-C8	118.8(2)
C8A-C8	1.430(3)	O1-C8-C7	121.6(2)
C4A-C5	1.418(4)	C7-C8-C8A	120.6(2)
C2-C3	1.398(4)	C4-C4A-C8A	117.4(2)
C13-C14	1.503(5)	C5-C6-C7	122.3(2)
C4-C3	1.357(4)	C6-C5-C4A	118.9(2)
C7-C8	1.373(3)	N10-C11-C12	111.7(2)
C7-C9	1.520(4)	C3-C4-C4A	119.7(3)
N10-C9	1.473(3)	C11-C12-C13	110.7(3)
N1-C2	1.326(4)	C13-C14-C15	111.4(3)
C8A-C4A	1.420(3)	C8-C7-C9	120.1(2)
C4A-C4	1.412(4)	C11-N10-C9	110.3(2)
C6-C5	1.369(4)	C9-N10-C15	110.8(2)
C11-C12	1.510(4)	N1-C8A-C4A	122.7(2)
C13-C12	1.518(5)	C4A-C8A-C8	118.6(2)
C15-C14	1.506(6)	O1-C8-C8A	117.8(2)
		C4-C4A-C5	122.4(3)
		C5-C4A-C8A	120.2(2)
		N10-C9-C7	112.7(2)
		N1-C2-C3	124.8(3)
		C14-C13-C12	109.7(3)
		N10-C15-C14	111.5(3)
		C4-C3-C2	118.6(3)

Table S3. Selected intra- and intermolecular X-H…Y interactions in **Q-3**.

X-H...Y	symmetry operation	X-H [Å]	H...Y [Å]	X...Y [Å]	X-H...Y [°]
O1-H1O…N10	intra	1.01(5)	1.67(5)	2.658(3)	164(4)
C2-H2…O1	2-x,-1/2+y,1/2-z	0.93	2.67	3.597(4)	177
C11-H11B…Cg(B)	-1/2+X,3/2-Y,1-Z	0.97	2.63	3.550(3)	159
C12-H12A…Cg(A)	1-X,-1/2+Y,1/2-Z	0.97	2.91	3.771(4)	149
C13-H13A…Cg(B)	1-X,-1/2+Y,1/2-Z	0.97	2.96	3.663(4)	130

Table S4. Bond lengths (Å) and angles (°) in **Q-4**·HCl·H_2O.

Bond lengths (Å)		angles (°)	
Cl1-C5	1.742(2)	C2-N1-C8A	117.4(1)
O1-C8	1.350(2)	N1-C2-C3	123.7(2)
N1-C8A	1.364(2)	C3-C4-C4A	119.6(2)
N10-C11	1.504(2)	C4-C4A-C8A	116.9(1)
C3-C4	1.354(3)	C6-C5-C4A	121.8(1)
C4A-C5	1.417(2)	C4A-C5-Cl1	119.2(1)
C5-C6	1.362(2)	C8-C7-C6	119.9(1)
C7-C8	1.372(2)	C6-C7-C9	120.1(1)
C8-C8A	1.424(2)	O1-C8-C8A	121.5(1)
C12-C13	1.378(2)	N1-C8A-C4A	122.8(1)
C13-C14	1.377(3)	C4A-C8A-C8	119.3(1)
C15-C16	1.375(3)	C12-C11-N10	112.6(1)
F1-C13	1.352(2)	C13-C12-C11	121.6(1)
N1-C2	1.322(2)	F1-C13-C14	118.3(2)
N10-C9	1.492(2)	C14-C13-C12	123.7(2)
C2-C3	1.401(2)	C14-C15-C16	120.7(2)
C4-C4A	1.416(2)	C16-C17-C12	120.9(2)
C4A-C8A	1.421(2)	C9-N10-C11	113.8(1)
C6-C7	1.412(2)	C4-C3-C2	119.5(2)
C7-C9	1.503(2)	C4-C4A-C5	125.1(1)

C11-C12	1.503(2)	C5-C4A-C8A	118.0(1)
C12-C17	1.387(2)	C6-C5-Cl1	119.0(1)
C14-C15	1.370(3)	C5-C6-C7	120.3(1)
C16-C17	1.381(3)	C8-C7-C9	119.9(1)
		O1-C8-C7	117.8(1)
		C7-C8-C8A	120.7(1)
		N1-C8A-C8	117.9(1)
		N10-C9-C7	111.7(1)
		C13-C12-C17	116.7(1)
		C17-C12-C11	121.7(1)
		F1-C13-C12	118.0(2)
		C15-C14-C13	118.0(2)
		C15-C16-C17	120.1(2)

Table S5. Selected intermolecular X-H…Y interactions in **Q-4**·HCl·H_2O.

X-H...Y	symmetry operation	X-H [Å]	H...Y [Å]	X...Y [Å]	X-H...Y [o]
N10-H10B…O1	Intra	0.89	2.72	3.2053(16)	115
O2-H2O…Cl2		0.85(3)	2.35(3)	3.1802(15)	168(3)
N10-H10A…O2		0.89	1.93	2.7923(18)	164
N10-H10B…Cl2	-1+x,y,z	0.89	2.36	3.1314(13)	145
O1-H1O…N1	-x,1-y,1-z	0.80(2)	2.15(2)	2.8073(18)	141(2)
O2-H2W…Cl2	1-x,1-y,-z	0.78(3)	2.37(3)	3.1397(17)	169(3)
C2-H2…O1	-x,1-y,1-z	0.93	2.50	3.001(2)	114
C14-H14…O2	x,-1+y,z	0.93	2.64	3.477(2)	150

Table S6. λ_{max} (nm) and molar absorptivity ($M^{-1}cm^{-1}$) values for the ligand species of the studied 8-hydroxyquinolines in the different protonation forms determined by UV–Vis spectrophotometric titrations, as well as the determined proton dissociation constants (pK_a). (T = 25 °C, I = 0.20 M (KCl))

	Q-1	**Q-2**	**Q-3**	**Q-4**
H_3L [b]	–	308 nm (2750)	–	–
		318 nm (2945)		
		336 nm (2120)		
H_2L [b]	308 nm (3320) [a]	302 nm (2420)	308 nm (2790)	326 nm (2800)
	318 nm (3420) [a]	424 nm (425)	320 nm (2970)	390 nm (730)
	358 nm (3370) [a]		340 nm (2190)	
HL [b]	306 nm (4914) [a]	312 nm (2360)	304 nm (2790)	342 nm (2370)
			428 nm (380)	402 nm (1580)
L [b]	334 nm (5560) [a]	338 nm (3760)	336 nm (4000)	342 nm (2080)
	354 nm (~5500) [a]	358 nm (2800)		398 nm (1400)
pK_1	4.99 [a]	2.59±0.05	2.69±0.02	5.16±0.05
pK_2	9.51 [a]	6.25±0.06	6.99±0.01	8.54±0.05
pK_3	–	10.37±0.06	–	–

[a] Data taken from Ref. [É. A. Enyedy, O. Dömötör, E. Varga, T. Kiss, R. Trondl, C. G. Hartinger and B. K. Keppler, J. Inorg. Biochem., 2012, **117**, 189–197.]
[b] Charges are omitted for clarity.

Table S7. λ_{max} (nm) and molar absorptivity ($M^{-1}cm^{-1}$) values for the iron(III) and copper(II) complexes of **Q-1** to **Q-4.** (T = 25 °C, I = 0.20 M (KCl)) (Charges of the complexes are omitted for clarity.)

	Q-1	**Q-2**	**Q-3**	**Q-4** [b]
[FeLH]	–	628 nm (630)	–	–
		452 nm (280)		
[FeL]	650 nm [a]	592 nm (884)	636 nm (1020)	–
		444 nm (1010)	456 nm (580)	
[FeL_2H_2]	–	–	–	–
[FeL_2H]	–		–	–
		604 nm (2535)		
		448 nm (1940)		
[FeL_2]	625 nm [a]	–	588 nm (2960)	–
			448 nm (3015)	
[FeL_3H]	–	576 nm (3750)	–	–
		452 nm (3973)		
[FeL_3]	575 nm [a]	576 nm (3750)	572 nm (4250)	–
		444 nm (4000)	440 nm (5200)	
[CuLH]	–	–	–	382 nm (2561)
[CuL]	–	374 nm (1980)	362 nm (1850)	426 nm (2252)
[CuL_2H_2]	–	–	–	390 nm (6397)
[CuL_2H]	–	372 nm (5793)	–	430 nm (5250)
[CuL_2]	–	382 nm (4970)	374 nm (5250)	–

[a] Data taken from Ref. [T. D. Turnquist and E. B. Sandell, Anal. Chim. Acta, 1968, **42**, 239–245.]
[b] No detectable CT or d-d bands, only ligand bands were used for calculations due to the highly diluted conditions.

Table S8. Anisotropic EPR parameters for *bis*-ligand copper(II) complexes of **Q-1**, **Q-2**, **Q-3** and **Q-4** in frozen solutions (77 K) [a]

Ligand		g_x	g_y	g_z	A_x /G	A_y /G	A_z /G	a_{Nx} /G	a_{Ny} /G	a_{Nz} /G	ratio %
Q-1	*monomer*	2.039	2.058	2.256	17	16	168	13.1 13.0	13.1 13.0	9.0 9.0	100
Q-2	*monomer*	2.040	2.044	2.235	28	5	184	14.0 14.0	14.0 14.0	9.1 8.6	100
Q-3	*monomer*	2.051	2.070	2.287	13	1	151	13.0 13.4	12.6 14.4	9.0 9.0	25
	dimer[b]	2.023	2.052	2.220	0	25	186				75
Q-4	*monomer*	2.051	2.070	2.287	13	1	151	13.0 13.4	12.6 14.4	9.0 9.0	10
	dimer[b]	2.023	2.052	2.220	0	25	186				90

[a] The experimental errors were ±0.001 for g_x, g_y and g_z, ± 1 G for A_x, A_y, A_z and a_{Nx}, a_{Ny}, a_{Nz}.
[b] Further EPR parameters used in the simulation: χ = 28.5°, ψ = -5.0°; dipolar coupling D = 335.5 G; spin-exchange coupling J> 1500 G; Euler angles α = 0°, β = 3.3°, γ = -5°. From the dipolar coupling the copper-copper distance 3.88Å can be calculated by using point-dipole approach.

Table S9. Selected intra- and intermolecular X-H…Y interactions in $[(Cu(H\mathbf{Q\text{-}2})_2)_2]\cdot(CH_3OH)_2\cdot Cl_4\cdot(H_2O)_2$.

X-H...Y	symmetry operation	X-H [Å]	H...Y [Å]	X...Y [Å]	X-H...Y [°]
C9-H9A…O1	Intra	0.97	2.52	2.913(5)	104
C29-H29B…O1	Intra	0.97	2.58	3.289(5)	130
C29-H29B…O11	Intra	0.97	2.53	2.889(5)	102
O6-H6O…Cl1		0.82	2.41	3.162(7)	152
N10-H10…Cl2		0.84(4)	2.27(4)	3.082(4)	165(4)
N30-H30…O5		0.94(5)	1.69	2.631(5)	176(4)
C11-H11B…Cl1		0.97	2.75	3.639(5)	153
C35-H35B…O6		0.97	2.33	3.285(9)	167
C14-H14A…Cl3		0.97	2.73	3.517(5)	139
C31-H31A…O13	1/2-x,-1/2+y,1/2-z	0.97	2.56	3.351(6)	138
O5-H5O…Cl3	x,-1+y,z	0.85(6)	2.21(6)	3.051(5)	167(6)

O5-H5W…Cl3	1/2-x,-1/2+y,1/2-z	0.88(5)	2.19(5)	3.059(5)	171(4)
C11-H11A…Cl3	1/2-x,-1/2+y,1/2-z	0.97	2.79	3.679(5)	153

Table S10. Selected intermolecular X-H…Y interactions in $[Cu(\mathbf{Q\text{-}3})_2]\cdot Cl_2$.

X-H...Y	symmetry operation	X-H [Å]	H...Y [Å]	X...Y [Å]	X-H...Y [°]
C2-H2…O1	Intra	0.97	2.68	3.139(12)	111
N10-H10…Cl1	1+x,y,z	0.98	2.12	3.085(8)	169
C14-H14B…Cl1		0.95	2.79	3.721(10)	162
C2-H2…Cl1		0.93	2.86	3.538(10)	130
C15-H15A…Cl1		0.97	2.85	3.760(12)	155

Table S11. Selected intermolecular X-H…Y interactions in $[Cu(H\mathbf{Q\text{-}4})_2(CH_3OH)]\cdot ZnCl_4\cdot CH_3OH$.

X-H...Y	symmetry operation	X-H [Å]	H...Y [Å]	X...Y [Å]	X-H...Y [°]
N10-H10B…O1	Intra	0.91	2.06	2.750(4)	132
N10-H10A…O4	1-x,2-y,-z	0.91	2.30	2.998(5)	133
O4-H2O…Cl5		0.86(8)	2.31(7)	3.135(4)	160(8)
O3-H3O…O4	1-x,2-y,-z	0.97(6)	1.80(6)	2.757(5)	166(6)
N10-H10A…Cl4	1-x,2-y,-z	0.91	2.55	3.254(4)	135
N10-H10A…O4	1-x,2-y,-z	0.91	2.30	2.998(5)	133
N30-H30A…Cl6		0.91	2.32	3.202(4)	165
N30-H30B…Cl5		0.91	2.58	3.218(4)	128
C23-H23…Cl6	1-x,1-y,-z	0.95	2.60	3.486(5)	155
C24-H24…Cl2		0.95	2.77	3.129(4)	103
C29-H29A…Cl3		0.95	2.73	3.647(4)	155
C31-H31A…Cl3		0.95	2.76	3.743(5)	172
C31-H31B…Cl6	1-x,1-y,-z	0.95	2.77	3.517(4)	133
C34-H34…F1	2-x,1-y,-z	0.95	2.31	3.143(6)	146
C39-H39A…Cl4		0.95	2.78	3.547(4)	135

Table S12. Electrochemical data (potentials *vs.* NHE) for the iron and copper complexes formed with ligands **Q-1** and **Q-3** in comparison to the metal chlorides (very low peak intensity was obtained for the **Q-2**[a] and **Q-4** complexes). (Glassy carbon working electrode, platinum counter electrode, Ag/AgCl/KCl (3 M) reference electrode; T = 25 °C; scan rate: 5 mV/s; I = 0.01 M ($TBAClO_4$); solvent: DMSO (H_2O content up to 1.64% for copper samples, 3.72% for iron samples); c_{ligand} = 1.0 mM)

	MCl_x	**Q-1**	**Q-3**
ligand signals			
E_a *vs*. NHE / V	-	-	-
E_c *vs*. NHE / V	-	-	-0.382[b]
[FeL_3] signals			
E_a *vs*. NHE / V	+0.435	-0.279	+0.126
E_c *vs*. NHE / V	+0.306	-0.367	-0.084
$E_{1/2}$ *vs*. NHE / V	+0.381	-0.323	+0.021
ΔE ($E_{1/2}$ complex – $E_{1/2}$ iron salt) / V	-	-0.704	-0.360
[CuL_2] signals			
E_a *vs*. NHE / V	+0.630	-0.431	-0.153
E_c *vs*. NHE / V	+0.521	-0.697	-0.257
$E_{1/2}$ *vs*. NHE / V	+0.576	-0.564	-0.205
ΔE ($E_{1/2}$ complex – $E_{1/2}$ copper salt) / V	-	-1.140	-0.781

[a] E_c *vs*. NHE of the ligand **Q-2**: -0.214 V.
[b] Broad peak.

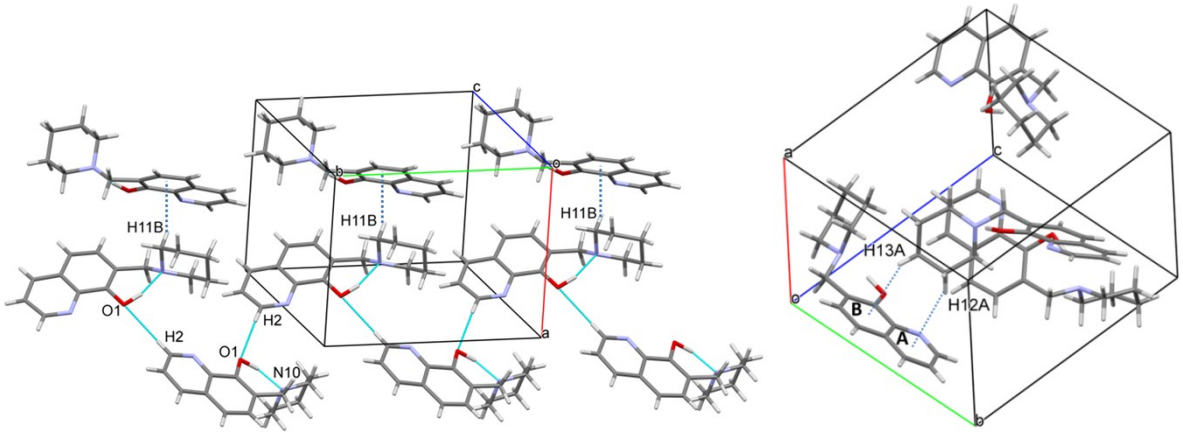

Figure S1. Packing arrangements in two different views showing selected intermolecular interactions in **Q-3**. Crystal data and structure refinement parameter for all crystals of this study are given in Table S1.

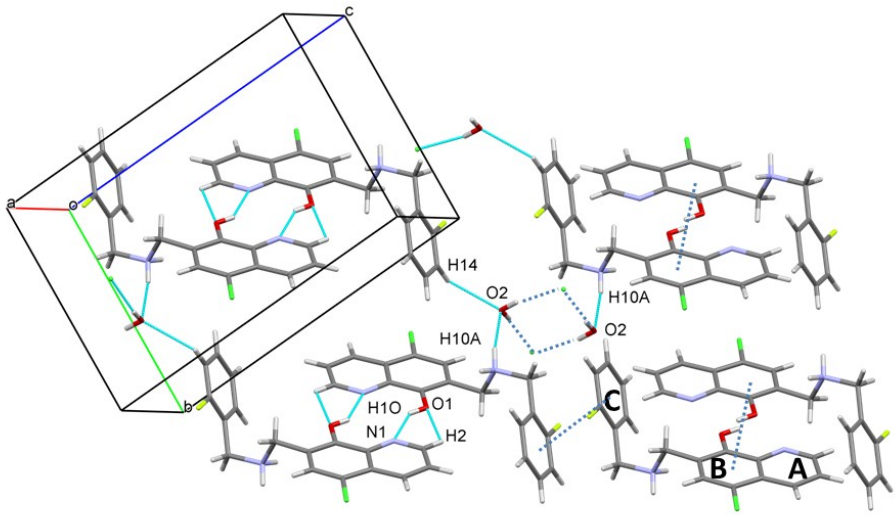

Figure S2. Packing arrangements showing selected X-H…Y and π…π interactions in **Q-4**·HCl·H_2O. Distance Cg(B)-Cg(B) is 3.7513(8) Å, Cg(C)-Cg(C) is 3.8244(11) and Cl1–Cl1 is 3.3506(7) Å. Crystal data and structure refinement parameter for all crystals of this study are given in Table S1.

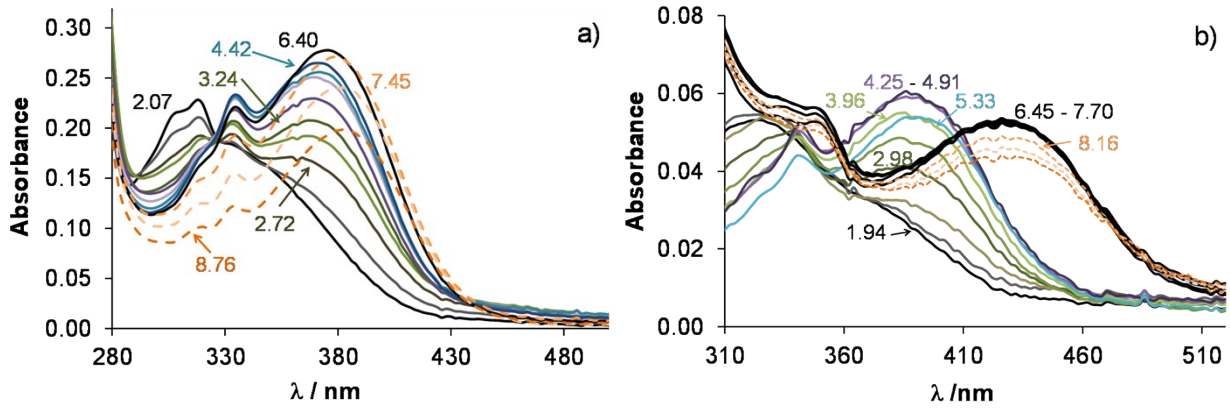

Figure S3. UV-Vis absorption spectra recorded for the copper(II) − **Q-2** (1:2) (a) and copper(II) − **Q-4** (b) systems at different pH values. (c_{ligand} = 50 μM (a) / 10 μM (b); T = 25.0 ˚C; I = 0.20 M KCl; l = 2 cm)

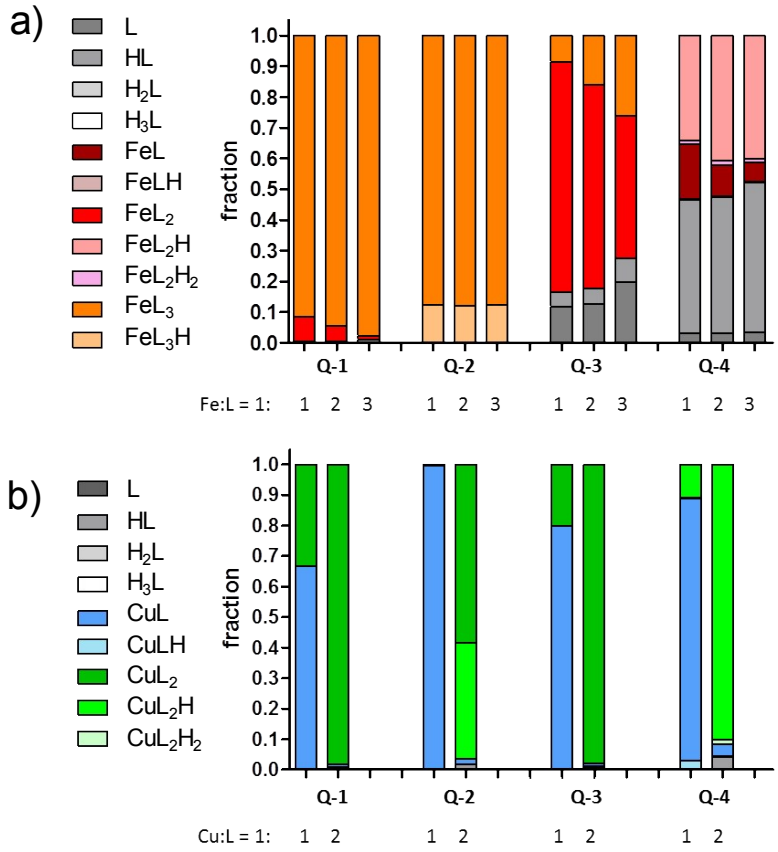

Figure S4. Ligand distribution at physiological pH at different metal-to-ligand ratios for iron(III) (a) and copper(II) (b) complexes. (c_{ligand} = 5 μM; T = 25.0 ˚C; I = 0.20 M KCl)

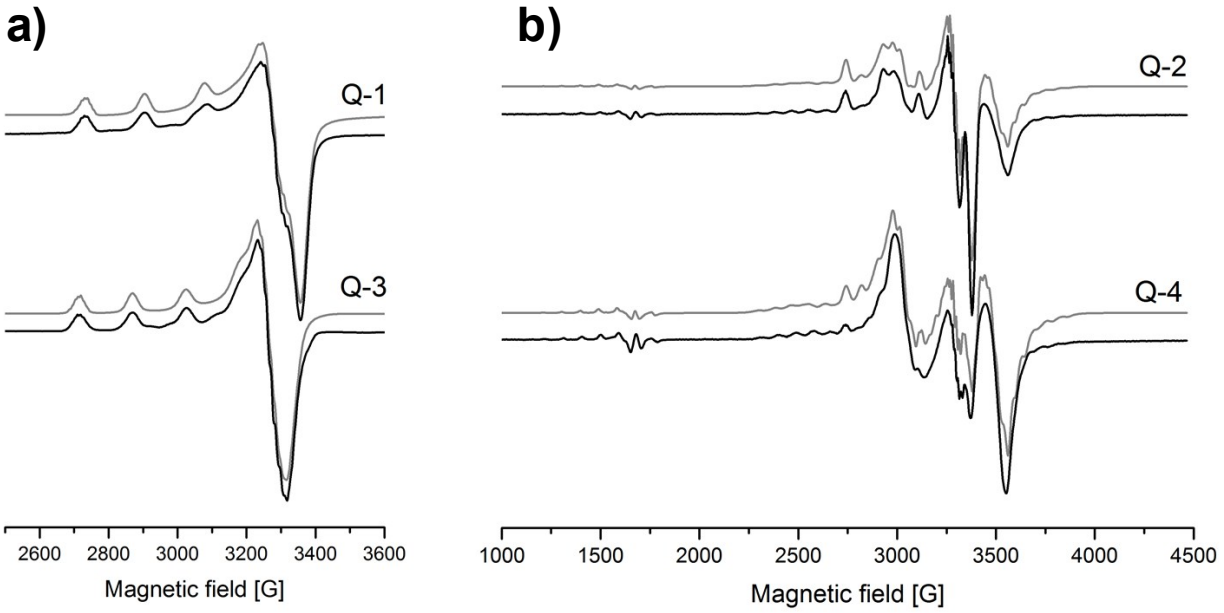

Figure S5. Experimental (black) and simulated (gray) EPR spectra recorded at 77 K (c_{Cu} = 2 mM, c_L = 4 mM) for copper(II) bis-ligand complexes of ligand **Q-1** (in toluene) and **Q-3** (in methanol) (a) and for **Q-2** and **Q-4** (in methanol) (a). EPR parameters are collected in Table S8.

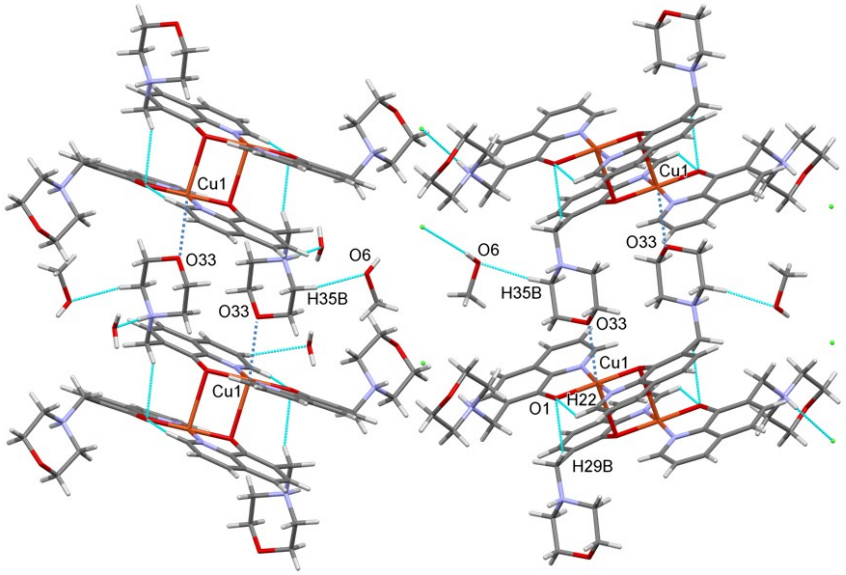

Figure S6. Packing arrangements showing Cu1-O33 close distance by dashed lines and selected X-H…Y interactions in $[(Cu(H\mathbf{Q\text{-}2})_2)_2]\cdot(CH_3OH)_2\cdot Cl_4\cdot(H_2O)_2$.

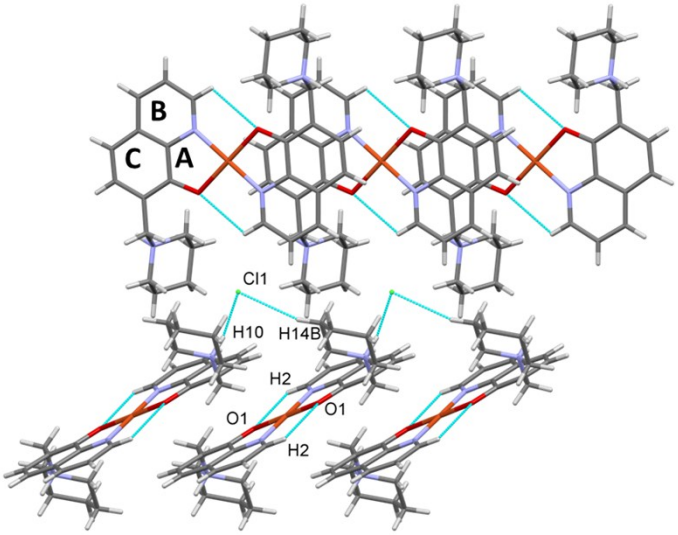

Figure S7. Packing arrangements showing selected C-H…Cl and C-H…O interactions in [Cu(**Q-3**)$_2$]·Cl_2. Distance Cg(A)-Cg(C) is 3.428(6) Å, Cg(B)-Cg(C) is 3.753(6) Å. Crystal data and structure refinement parameter for all crystals of this study are given in Table S1.

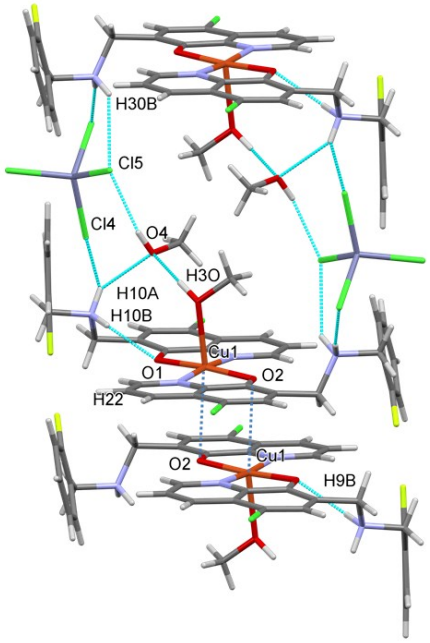

Figure S8. Packing arrangements showing selected X-H…Y interactions in [Cu(H**Q-4**)$_2$(CH_3OH)]·$ZnCl_4$·CH_3OH. Distance C1-O2 is 3.301(3) Å. The shortest F1-F2 distance is 3.126(5) Å, and copper-copper distance is 3.8354(8) Å. Crystal data and structure refinement parameter for all crystals of this study are given in Table S1.

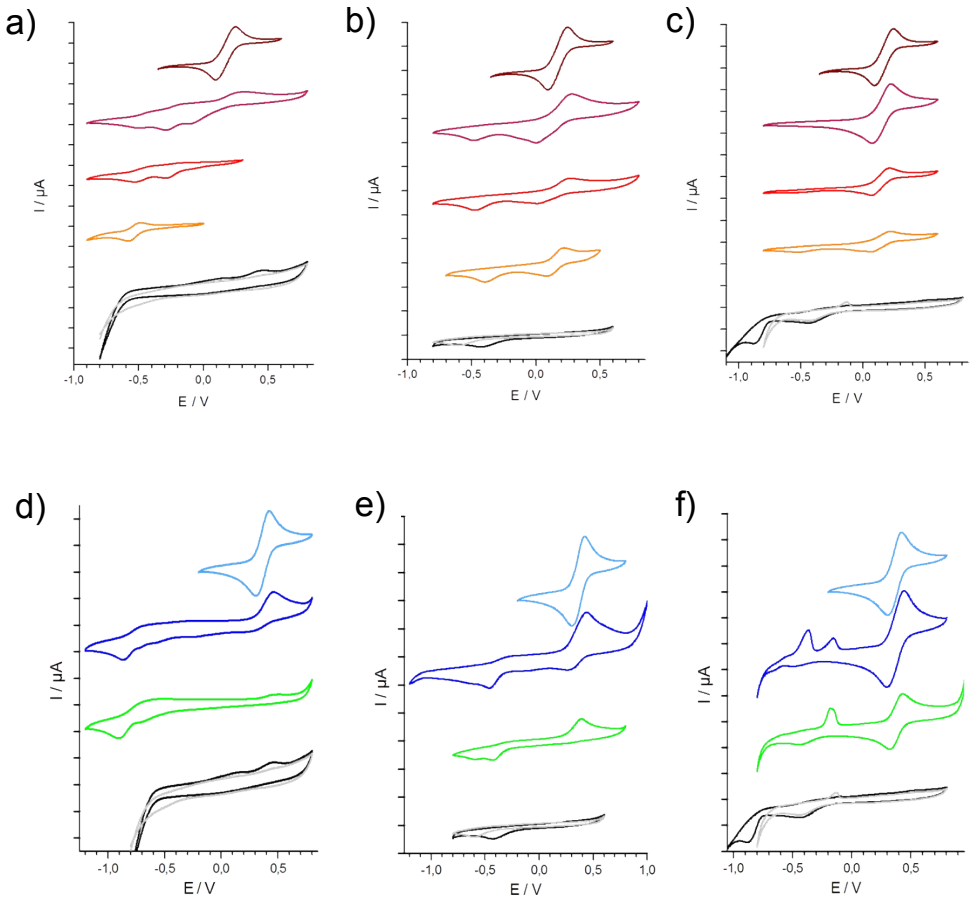

Figure S9. Cyclic voltammograms of the iron(III) – **Q-1** (a), iron(III) – **Q-2** (b), iron(III) – **Q-4** (c), copper(II) – **Q-1** (d), copper(II) – **Q-2** (e) and copper(II) – **Q-3** (f) systems. Ligand alone (black / deprotonated: grey), $FeCl_3$ (brown), iron complexes at the M:L ratios 1:1 (bordeaux), 1:2 (red) and 1:3 (orange), as well as for $CuCl_2$ (light blue), and copper complexes at the M:L ratios 1:1 (blue) and 1:2 (green). (Potentials measured against Ag/AgCl/KCl (saturated); c_{ligand} =1.0 mM; solvent: DMSO (with a H_2O content of up to 1.6% for copper samples and 3.7% for iron samples); I = 0.01 M ($TBAClO_4$); T = 25 °C; scan rate = 5 mV/s)

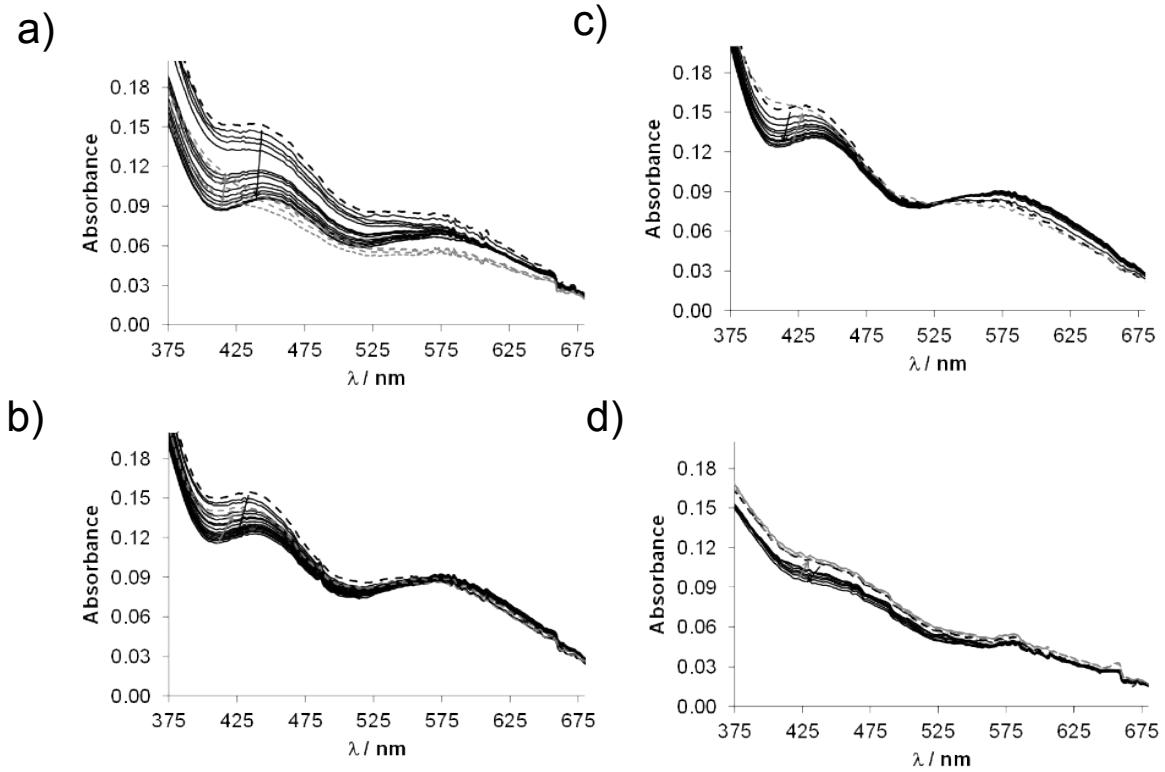

Figure S10. Time-dependent UV–Vis spectra of the iron(III) complexes of **Q-1** (b), **Q-2** (b), **Q-3** (c) and **Q-4** (d) upon addition of 2.5 equivalents of ASC at pH 6.87. Black dashed lines denote the initial spectra before addition of ASC, grey dashed lines the spectra upon addition of H_2O_2. ($c_{\text{iron(III)}}$ = 200 μM; c_{ligand} = 200 μM; c_{ASC} = 500 μM; T = 25.0 °C; I = 0.10 M KCl)

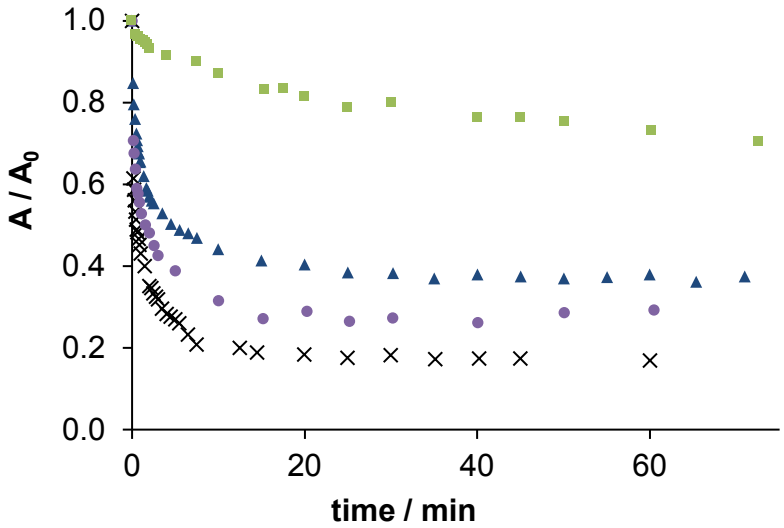

Figure S11. Absorbance changes (as A/A_0) at the λ_{max} of the copper(II) complexes upon reaction with 2.5 equivalents of GSH plotted against the time for the complexes of **Q-1** (●), **Q-2** (×), **Q-3** (▲) and **Q-4** (■) at pH 7.40. ($c_{copper(II)}$ = 100 μM; c_{ligand} = 100 μM; c_{GSH} = 250 μM; T = 25.0 ˚C; I = 0.10 M KCl)

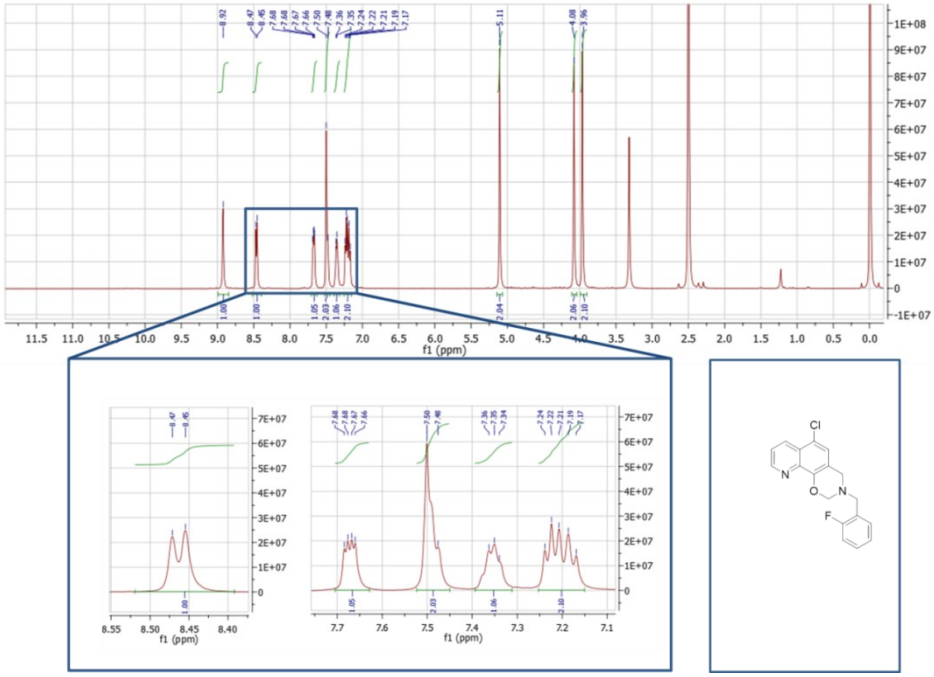

Figure S12. ^{1}H NMR spectrum of 6-chloro-3-(2-fluorobenzyl)-3,4-dihydro-2H-[1,3]oxazino[5,6-*h*]quinoline (NSC297366) in DMSO-d_6.

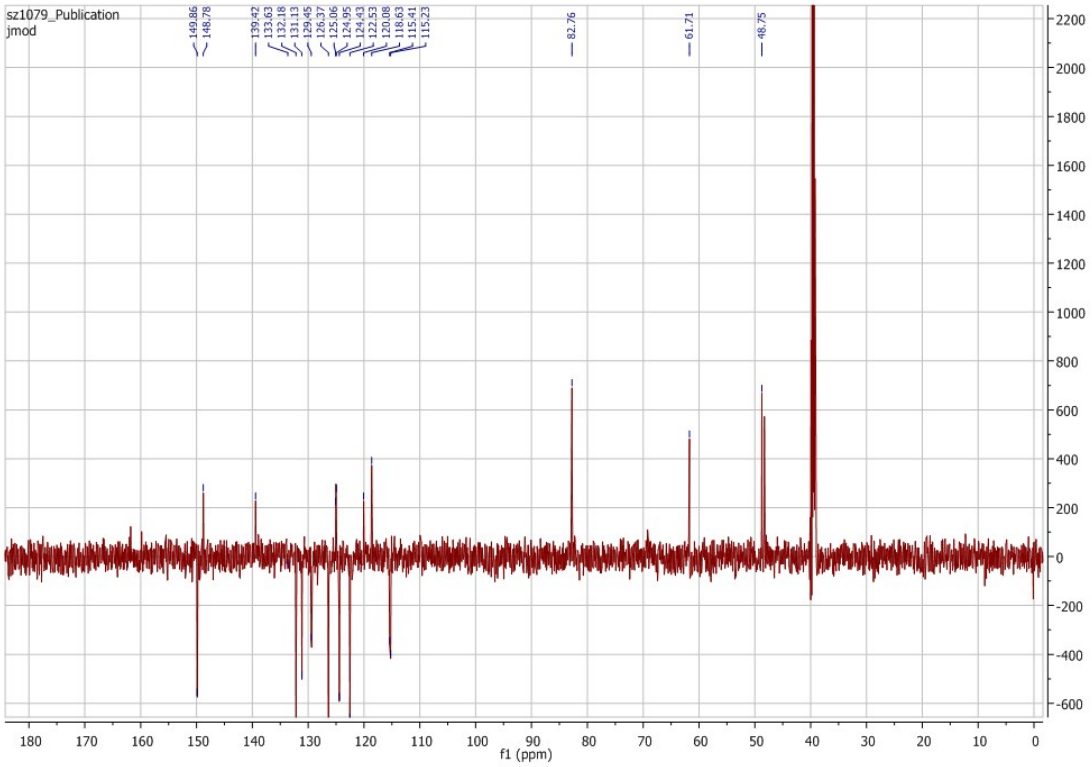

Figure S13. ^{13}C NMR spectrum of 6-chloro-3-(2-fluorobenzyl)-3,4-dihydro-2H-[1,3]oxazino[5,6-*h*]quinoline in DMSO-d_6.

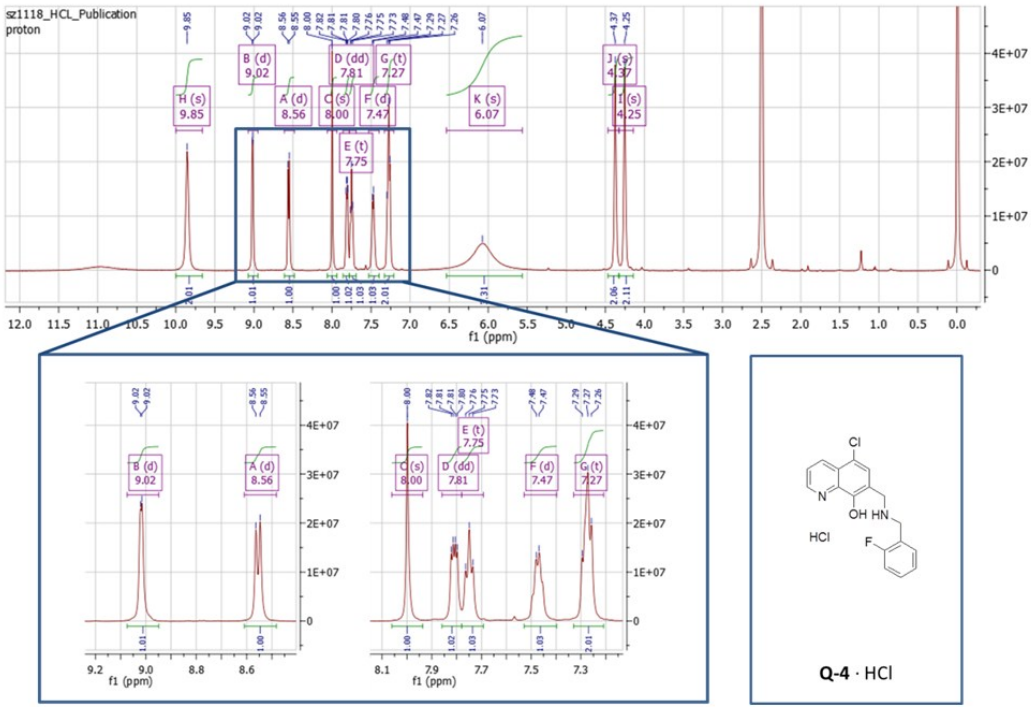

,

Figure S14. ^{1}H NMR spectrum of 5-chloro-7-((2-fluorobenzylamino)methyl)quinolin-8-ol hydrochloride (**Q-4**·HCl) in DMSO-d_6.

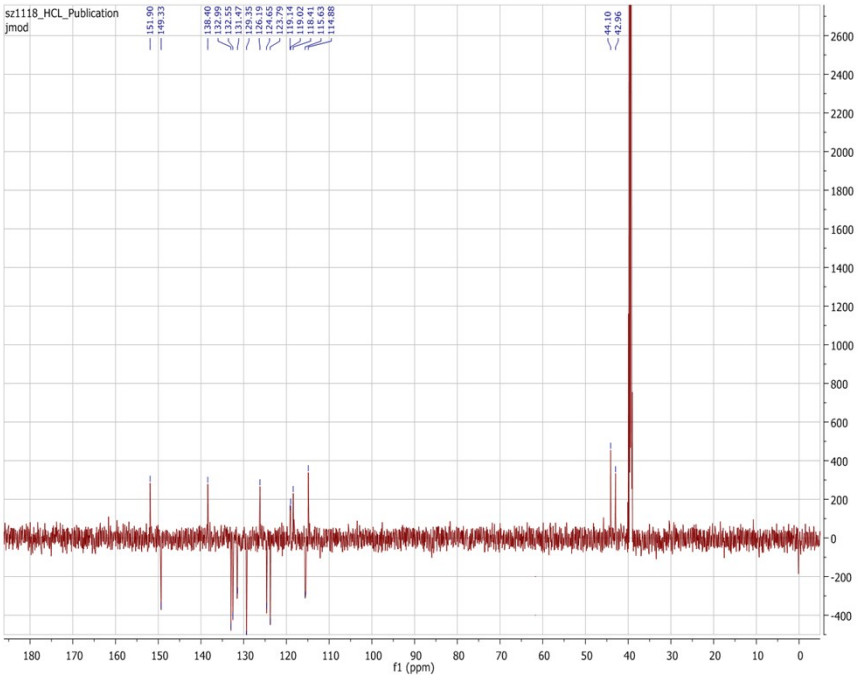

Figure S15. ^{13}C NMR spectrum of 5-chloro-7-((2-fluorobenzylamino)methyl)quinolin-8-ol hydrochloride (**Q-4**·HCl) in DMSO-d_6.